Longitudinal-optical phonons in thin films of rubidium iodide, potassium iodide, rubidium bromide, cesium iodide, and cesium bromide

T. G. Fiske and L. B. Coleman
Department of Physics, University of California, Davis, Davis, California 95616-8677
(Received 18 April 1991)

We have used the technique of far-infrared reflection-absorption spectroscopy to study the lattice dynamics of thin (60- to 3270-Å) films of rubidium iodide, potassium iodide, rubidium bromide, cesium iodide, and cesium bromide. The spectra provide information on the LO-phonon spectra as well as insight into the morphology of the thin-film samples.

I. INTRODUCTION

For many years far-infrared spectroscopy has been applied in the study of lattice dynamics of solids; however, attempts to examine the far-infrared spectra of thin films have been hampered by the lack of sensitivity of conventional far-infrared spectroscopies to submicrometer-thickness films. Recently, Da Costa has extended the technique of reflection-absorption spectroscopy into the far infrared.[1–4] As developed in our laboratory, far-infrared reflection-absorption spectroscopy (FIRRAS) has increased the sensitivity and dynamic range of far-infrared spectroscopy of dielectric films deposited on metal substrates. FIRRAS provides a direct measure of the ($q \approx 0$) LO phonon. Using this technique we have studied the effects of sample thickness and morphology on the lattice dynamics of the thin films of rubidium iodide, potassium iodide, rubidium bromide, cesium iodide, and cesium bromide.[5,6]

Excitation of the longitudinal-optical phonon is not allowed in the spectroscopy in bulk materials; however, Berreman[7] modeled the infrared (1000–2000 cm^{-1}) transmission and reflection of thin films (2500–3500 Å) of LiF and found that surface modes with frequencies characteristic of the longitudinal-mode frequency of LiF can be excited by non-normally-incident radiation polarized parallel to the plane of incidence (*p*-polarized radiation). These modes, which are not directly observable in a bulk crystal, are readily observed in a non-normal transmission or reflection-absorption measurement if the wavelength of the radiation is large compared to the thickness of the film.

For dielectric films deposited on a metal substrate, Berreman[7] found that at non-normal incidence, not only does one obtain an absorption at the LO-mode frequency, but the TO-mode absorption is practically eliminated from the spectrum when the film thickness is much less the wavelength of the incident radiation. This effect was later noted by Greenler[8] and is the basis for the surface specificity of reflection-absorption spectroscopy. The high conductivity of the metal substrate prohibits a parallel component of the electric field from existing near the surface, but enhances the component of the electric field perpendicular to the surface, with the result that the incident radiation can couple to vibrational modes with dipoles perpendicular, but not parallel, to the film surface. This has become known as the surface-dipole selection rule.

In addition to observing the LO phonon, we found spectral features that we attribute to the morphology of the thin films. As prepared in our laboratory, the alkali-halide films grow via a nucleative process, creating islands that grow to form a thin film. This creates voids in the film where the islands do not completely coalesce. The frequency and size of these additional spectral features depend on the volume fraction of the voids in the film and the geometry of the voids. We model the FIRRAS spectra of the alkali-halide films by combining an effective-medium approximation model with the classical Lorentzian oscillator model and our model of the electrodynamics of the FIRRAS process. From this model we are able to study both the effects of sample thickness and sample morphology on the longitudinal-phonon spectra of the films.

II. THE EFFECTIVE-MEDIUM APPROXIMATION

The optical properties due to the sample morphology of thin films is generally modeled in one of two ways. One can consider a rough film surface and modify the Fresnel amplitude reflection coefficient to describe this surface.[9–15] Alternatively, the dielectric response function of the film can be modeled by the inclusion of voids.[16–19] We have chosen the latter viewpoint, as our characterization of the films shows a film surface too smooth to cause the spectral features seen. We have developed an effective-medium-approximation (EMA) model to describe our films. The EMA is often used to describe the optical and electrical transport properties of heterogeneous media.[20–28]

We consider the thin-film system to be a flat smooth alkali-halide slab permeated by a distribution of aligned ellipsoidal voids of different shapes, with the total distributed volume of each shape taking up a small volume fraction of the total film volume (Fig. 1). As the thickness of the film is much less than a wavelength of the incident radiation, the model is not sensitive to the position of the voids in the film or to the size of individual voids.

 ©1992 The American Physical Society

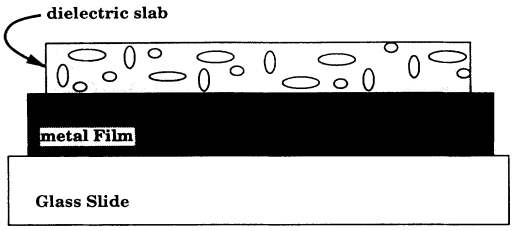

FIG. 1. Schematic representation of film samples with ellipsoidal voids.

Using the usual three-parameter Lorentzian oscillator model for the vibrational modes of the film, the dielectric response of the film material is

$$\epsilon(\omega)=\epsilon_\infty+\sum_{j=1}^{p}\frac{S_j}{\omega_{0j}^2-\omega^2-i\gamma_j\omega}\ , \tag{1}$$

where $\epsilon(\omega)$ is the complex dielectric function, ϵ_∞ is the high-frequency dielectric constant, p is the number of vibrational modes, S_j is the oscillator strength of the jth mode, ω_{0j} is the TO-mode frequency of the jth mode, and γ_j is the width of the jth mode.

We have constructed an EMA model of our thin dielectric films following the theory for the optical properties of small particles developed by Ruppin and Englman.[29] Consider an ellipsoid of material with a dielectric constant ϵ_e and a depolarization factor L_e embedded in a uniform isotropic medium with dielectric constant ϵ_m (we have dropped the explicit frequency dependence for clarity). For a film made up of the medium and a volume fraction f of aligned ellipsoids, the average dielectric function ϵ is[21,30]

$$\epsilon=\epsilon_m+\frac{f(\epsilon_e-\epsilon_m)}{1+(1-f)[(\epsilon_e-\epsilon_m)/\epsilon_m]L_e}\ . \tag{2}$$

Rearranging Eq. (2), we find

$$\frac{\epsilon-\epsilon_m}{L_c\epsilon+(1-L_c)\epsilon_m}=f\frac{\epsilon_e-\epsilon_m}{L_e\epsilon_e+(1-L_e)\epsilon_m}\ . \tag{3}$$

This is the form cited by Landauer[25] and used by Cohen *et al.*[23] to describe a heterogeneous medium consisting of a volume fraction f of aligned ellipsoids with dielectric constant ϵ_e and depolarization factor L_e embedded in a host of dielectric constant ϵ_m. We have labeled the L's in Eq. (3) to emphasize their origin. L_e on the right-hand side of Eq. (3) describes the shape of the particle or inclusion. L_c on the left-hand side of Eq. (3) describes the shape of the cavity used in the derivation of the Maxwell-Garnett EMA. It is essentially the fictitious Lorentz cavity used in the derivation of the local-field approximation. For the standard Maxwell-Garnett EMA, the Lorentz cavity and the inclusion are both spherical so that $L_c=L_e=\frac{1}{3}$. In a similar analysis, Galeener[18,19] derived an EMA to describe the optical properties of crack-like voids in amorphous germanium.

To provide for ellipsoidal inclusions of different shapes in our thin-film geometry, we set $L_c=1$, sum over the different shapes, and rewrite Eq. (3),

$$\epsilon=\epsilon_m\left[1-\sum_i f_i\frac{\epsilon_e-\epsilon_m}{L_{e_i}\epsilon_e+(1-L_{e_i})\epsilon_m}\right]^{-1}\ , \tag{4}$$

where f_i is the volume fraction of an ellipsoidal void with depolarization factor L_{e_i}. For one ellipsoid shape and small $\sum_i f_i$, Eq. (4) approximates Eq. (2), the basic form of the EMA.

III. EXPERIMENTAL DETAILS

The FIRRAS spectrometer is a double-polarization modulation modification of a Martin-Puplett configuration interferometer. Details of the technique and principles of FIRRAS are found elsewhere.[1–4,31] Spectra were obtained with a resolution of 1.9 cm^{-1}.

The FIRRAS sample chamber is evacuated to a base pressure below 5×10^{-5} Torr using a mechanical-pump-backed diffusion pump. A liquid-nitrogen-cooled trap in the sample chamber further reduces condensables. The pressure of the sample box is monitored by both a thermocouple and ionization tube. A single sample holder was built to control the temperature of the sample from 85 to 300 K. The sample holder has been described elsewhere.[1,2,5]

Five materials were studied: rubidium iodide, potassium iodide, rubidium bromide, cesium iodide, and cesium bromide. All materials were obtained from CERAC, Inc., and were typically 99.9% pure. The substrates were aluminum-coated glass microscope slides. The aluminum was evaporatively deposited to thicknesses between 0.5 and 1.0 μm. The alkali-halide thin films were produced by thermal evaporation at pressures less than 10^{-6} Torr. The thickness was controlled by evaporating a measured amount of material at a specific distance from the substrate and assuming a spherical distribution of evaporant. As these materials are hygroscopic, care was taken in their handling and storage.

After spectroscopic measurements were made, the films were characterized by four methods. The thickness was measured with a Sloan DEKTAK 3030 profilometer. The profilometer is accurate to within approximately 20 Å. The crystalline orientation was established by x-ray diffraction. Table I details the thickness, thickness standard deviation, and crystalline orientation of each sample. The RbI, RbBr, and KI films which have the NaCl structure, are oriented with the [100] direction perpendicular to the substrate. The CsI and CsBr, which have the CsCl structure, are oriented with the [110] direction perpendicular to the substrate. One film was studied using scanning electron microscopy (SEM). A reproduction of the SEM micrograph of the 1100-Å RbI film is shown in Fig. 2. The nucleative nature of film growth produces islands that incompletely grow together to form the gaps seen in Fig. 2.

The density was approximated from the film's volume and mass. Two measurements of a 1300-Å-thick RbI film gave values between $3\pm6\%$ and $6\pm10\%$ less than the density of bulk RbI. The large uncertainties of approximately 6–10% arise from the small mass of the films.

TABLE I. Alkali-halide thin films.

Material	Thickness (Å)	Thickness standard deviation (Å)	Crystalline orientation
RbI	60	20	[100]
	120	20	
	220	40	
	350	30	
	1100	40	
	3500	60	
KI	700	25	[100]
RbBr	570	30	[100]
CsI	700	25	[110]
CsBr	670	20	[110]
	3270	40	

While not precise, these measurements establish a range for the void volume parameters used to fit the spectroscopic data. The SEM micrographs give only the lateral dimensions of the film's islands and the profilometer does not have sufficient lateral resolution to determine the depth profile of the film surface. Samples that were characterized by atomic-force microscopy showed that the film surface is relatively flat over large areas compared to the size of the gaps between the crystallites.

IV. SPECTRAL ANALYSIS

To interpret the FIRRAS spectra we have modified the analysis software developed by Da Costa and Coleman[4] to include the EMA model with up to five different void shapes and volume fractions in addition to the classical Lorentzian mode parameters of frequency, strength, and width for each mode in the bulk material. Modeling the electrodynamics of FIRRAS using a three-layer system (air-film-metal substrate), the spectra will depend on the incident angle, the film thickness, the complex index of the substrate, and the complex index of the film. The frequency-dependent dielectric function of the thin film is derived by adjusting the parameters of the Lorentzian oscillator, Eq. (1), and the EMA model, Eq. (4). The resulting dielectric-function model is then used to determine the FIRRAS absorbance. We use a unitless FIRRAS absorption function similar to the one defined by Greenler:[32]

$$A(\omega)_{(p,s)}=1-\frac{R_{0(p,s)}-R_{(p,s)}}{R_{0(p,s)}}=\frac{R_{(p,s)}}{R_{0(p,s)}}\ , \tag{5}$$

where $R_{0(p,s)}$ are the measured reflectivities of the bare and film covered metal substrate, respectively, and p (s) refers to light polarized perpendicular (parallel) to the substrate. The reflectivities are obtained from the Fresnel coefficients of the air-film and film-substrate interfaces, which in turn depend on film thickness, angle of incidence, and the complex dielectric functions of the film and substrate. Details are given elsewhere.[4]

For our analysis, the substrate index was taken to be equal to the refractive index of bulk aluminum at 400 cm^{-1}. The index of aluminum does have a slight frequency dependence over the spectral range of the FIRRAS experiment; however, the spectra are independent of the substrate index as long as the dielectric constant of the metal substrate is much greater than that of the deposited dielectric film, and the film thickness is much smaller than the wavelength of the incident light. To apply our EMA model to the thin-film system, we set ϵ_m equal to the bulk dielectric function of the alkali halide and $\epsilon_e=1$ for a void.

As noted by Berreman[7] and others,[4,33,34] the spectra obtained by oblique angle reflectance from thin absorbing films on metal substrates is approximately proportional to $-\omega\,\mathrm{Im}[1/\epsilon(\omega)]$, where $\epsilon(\omega)$ is the dielectric function of the absorbing film. Maxima in the spectra appear at the minima of $\epsilon(\omega)$. These will occur in our EMA ϵ at the zeros of $\epsilon_m(\omega)$ (i.e., at $\omega=\omega_{\mathrm{LO}}$) and when the term in the denominator of the summed term in Eq. (4) is a minimum. This last condition yields

$$\frac{\omega_{Vi}^2}{\omega_{\mathrm{LO}}^2}=\frac{\epsilon_{m_\infty}}{\epsilon_m(0)}\,\frac{\epsilon_m(0)-1(1-1/L_i)}{\epsilon_{m_\infty}-1/(1-1/L_i)}\ . \tag{6}$$

This equation predicts that each void shape will give rise to an absorption peak with a frequency ω_{Vi} such that $\omega_{\mathrm{TO}}<\omega_{Vi}<\omega_{\mathrm{LO}}$, where ω_{Vi} depends on the shape of the void. We refer to these spectral features as void resonances after Galeener.[18,19]

One interesting characteristic of FIRRAS has been pointed out by Da Costa and Coleman.[4] For a dielectric function containing two neighboring modes, the modes will "repel" each other with the lower (higher) frequency mode shifting to lower (higher) frequency. In addition the peak height of the lower (higher) frequency mode will be reduced (increased) by a factor proportional to the oscillator strength of other mode. The net effect is that the

FIG. 2. Scanning electron micrograph of RbI film. Magnification is times 11 380. Bar represents 8790 Å.

effective oscillator strength from the lower-frequency mode shifts into the effective oscillator strength of the higher-frequency mode. For the alkali halides studied here, this phenomenon is seen as an increase in the oscillator strength of phonon sum modes at the expense of the LO-phonon mode. Without this effect, the phonon sum modes would not be observable.

V. RESULTS AND DISCUSSION

Common features are seen in all of the alkali-halide films studied. We will discuss the rubidium-iodide results in detail and conclude with a summary of the results of the other materials. The FIRRAS spectra of an 1100-Å thick film of RbI are displayed in Fig. 3. As described above, maxima in the FIRRAS signal appear at zeros of the dielectric function, leading to FIRRAS maxima at the LO-phonon frequency. In Fig. 3, the major feature at 99 cm^{-1} (all observed frequencies are reported to within 1 cm^{-1}) is the LO-phonon absorption. The higher-frequency feature (111.5 cm^{-1} arises from a two-phonon summation mode. As the temperature is lowered, the LO-mode frequency increases and the mode width decreases. The summation mode becomes less evident, and below 200 K new features appear below the LO-mode frequency. We ascribe these features to sample morphology. These spectra are typical of all the films studied, with the number of high-frequency summation bands and low-frequency sample morphology features varying with the material studied.

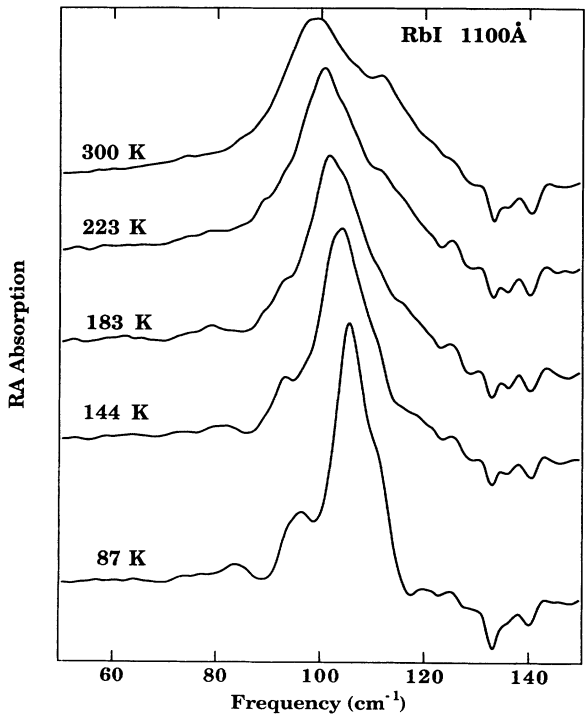

FIG. 3. Temperature dependence of FIRRAS spectra of 1100-Å RbI film. Spectra are displaced for clarity.

To obtain the frequency-dependent optical constants of the films, we fit the FIRRAS spectra using the three-parameter Lorentzian oscillator-EMA model described in Secs. II and IV. The spectral fits are produced by first assigning values for the TO frequency and oscillator strength of each vibrational feature (i.e., the TO mode and the sum modes). The phonon (TO) frequency and high-frequency dielectric constant are taken from the work of Lowndes and Martin[35] and Lowndes.[36] The initial values of the TO-mode frequencies at lower temperatures were obtained from interpolation between the room-temperature value and the experimental value at 80 K, with the final TO frequency values coming from the fitting procedure. The TO frequencies of the sum modes

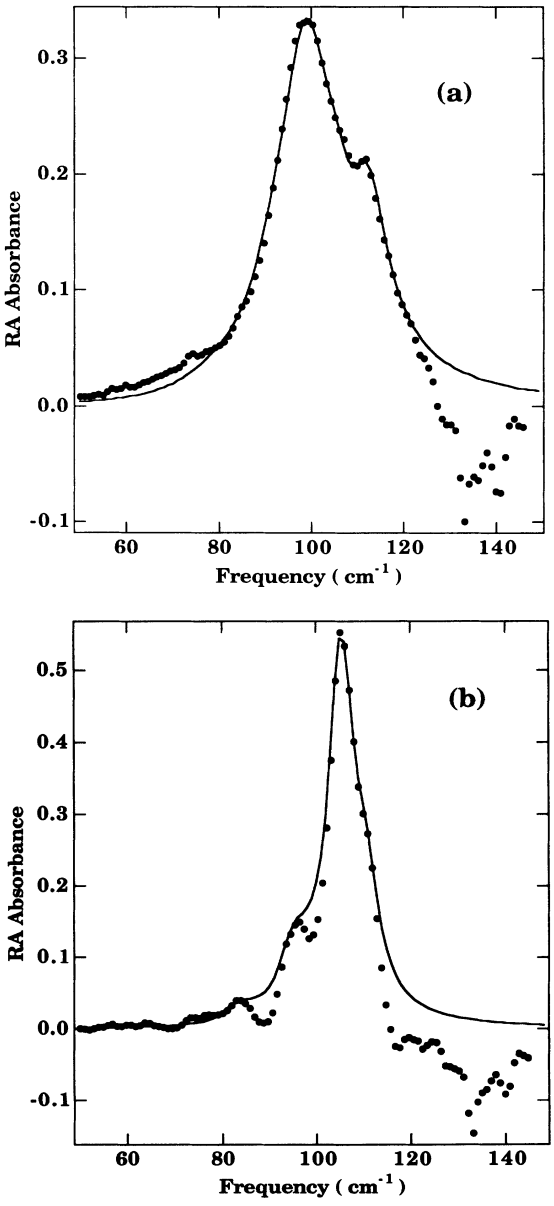

FIG. 4. FIRRAS spectra and model analysis of 1100-Å film of RbI at (a) 300 and (b) 90 K. Measured spectra, dots; model analysis, solid line.

are visually estimated. The shape of each LO mode was modeled by adjusting the damping parameter. The sample-morphology features were modeled by adjusting the void parameters in the EMA. The void resonance frequency is determined primarily by the void shape, while the relative height of the feature is determined by the volume fraction of the void. The absolute FIRRAS absorption was matched by slight adjustments of the angle of incidence. The fitting procedure is iterative, with visual comparison of the data and the calculated spectrum and modification of the parameters until a satisfactory fit is achieved. The LO-phonon frequencies are obtained from the peaks of the $\mathrm{Im}(1/\epsilon)$ curve and are accurate to within 1 cm^{-1}. The peak positions of the FIRRAS spectra and the $\mathrm{Im}(1/\epsilon)$ curve coincide to within 1 cm^{-1}, and in most cases there is no difference. Typical results of the fitting procedure are shown in Figs. 4(a) and 4 (b). Further details of the fitting procedure have been presented elsewhere.[4,5]

A. Rubidium iodide

The FIRRAS spectra of the 1100-Å RbI sample was modeled by three independent oscillators and a uniform distribution of voids with two different shapes. Table II compares the current measurement of the LO frequency with similar previous measurements. The FIRRAS-derived LO-mode frequency of 99 cm^{-1} at room temperature is compared to 97.5 cm^{-1} reported by Lowndes.[36] Our temperature-dependent LO frequencies are generally 1.0–1.5 cm^{-1} higher than those reported by Lowndes. Comparisons with other measurements are also shown in Table II.

Our results can also be examined by comparison with FIRRAS spectra calculated from optical constants derived from bulk samples. FIRRAS spectra can be simulated via Eq. (5) using the bulk RbI optical constants of Pai *et al.*,[37] the measured film thickness and the appropriate angle of incidence. The measured FIRRAS spectra are broader and have slightly lower intensities than the simulated FIRRAS spectra at room temperature. The LO-mode frequencies from the simulated (99 ± 1 cm^{-1}) and measured (99 cm^{-1}) FIRRAS spectra agree. Phonon summation modes are observed in the simulated FIRRAS spectra. In addition to the phonon sum mode at 111.5 cm^{-1}, a sideband shoulder is seen at 122 cm^{-1} in the simulated FIRRAS spectra. While this additional summation band is not observed in the 1100-Å film, it is seen in thicker (2500-Å) films. At 100 K the sample-morphology features are clearly resolved from the LO mode in the measured FIRRAS spectra, and the shape of the reststrahlen mode agrees well with that of the simulated FIRRAS spectra at 100 K. This suggests that the increased linewidth (decreased lifetime) of the thin-film spectra most likely follows from the sample morphology and higher concentrations of defects and grain boundaries in the film as compared to the bulk material. Similar results are seen in the comparisons between simulated and measured spectra for other thicknesses of RbI films and for KI and RbBr films.

The TO- and LO-mode frequencies, linewidths, and oscillator strengths as a function of temperature are given

TABLE II. Measured and calculated LO-phonon frequencies (in cm^{-1}). The uncertainty in all frequency values is ±1 cm^{-1} except as noted.

			Lowndes[a]				
Material	Thickness (Å)	FIRRAS	Grazing angle measurement	Bulk measurement	Simulated FIRRAS	LST[b]	Neutron scattering
RbI	2500	99	97.5±0.5	95±0.5	98	100	100±2[c]
	1100	99				99	
	350	98				101	
	210	98				96	
	120	95.5				98	
	60	90.5				100	
KI	700	131	127±0.5	129±0.5	131	40	142±3[d]
RbBr	570	122	128±0.5		119	123	129±3[e]
CsI	700	90	90.5±0.5	90.5±0.5		92	87[f]
CsBr	3270	116.5	113±0.5			112	111[g]
	670	115				113	

[a]Reference 36.
[b]Generalized Lyddane-Sachs-Teller (LST) relation.
[c]Reference 43; at 300 K.
[d]Reference 48; at 95 K.
[e]Reference 49; at 80 K.
[f]Reference 50; 300 K (estimated).
[g]Reference 51; at 80 K (estimated).

in Table III. The shift of the LO-mode frequencies that we observe with temperature follows from lattice thermal expansion and cubic and quartic anharmonic interactions.[38] These contributions to the frequency shift raise the mode frequencies linearly with decreasing temperature between 100 and 300 K. The LO-mode linewidth differs from the TO-mode linewidth because of the frequency dependence of the mode width. The peak height of the LO mode increases slightly with decreasing temperature, while the peak height of the high-frequency sidebands decreases slightly. This is reflected in the relative change in oscillator strength between the modes (Table III). The total oscillator strength is conserved. All of these effects are as expected from the usual understanding of the lattice dynamics of these ionic materials.

The high-frequency sidebands arise from anharmonic interactions between phonons. The anharmonic features of the absorption spectra of crystals are often modeled by using a frequency-dependent mode width calculated from a specific anharmonic model of the lattice potential. Such calculations have been carried out for the alkali halides by Hardy and Eldridge and their co-workers.[39–41] The resulting frequency-dependent mode width varies strongly with frequency. Below ω_{TO}, the damping is due to two-phonon difference processes, with summation processes dominating above ω_{TO}. This strong variation of the mode width with frequency contributes to the observed sideband structure of the optical absorption in these materials.[38] We model these phonon combination processes by adding independent classical oscillators with frequency-independent mode widths to the dielectric function used to calculate the FIRRAS spectra. This yields good fits to the data; however, one must not attach too much quantitative significance to the resulting mode parameters; there is only one fundamental lattice vibrational mode in these materials—the additional high-frequency features arise from anharmonic effects.

The summation modes seen above the LO mode are due to combinations of two phonons such that the total wave vector of the combination is zero or equal to a reciprocal lattice vector. The observable combinations are also restricted by group-theoretical considerations[42] and the form of the third-order potential term that couples the LO mode to any other two phonons.[40] We make tentative assignments of the sidebands using published inelastic neutron-scattering data.[43] The larger sideband near 111 cm^{-1} is assigned to the combinations at the $L[\frac{1}{2},\frac{1}{2},\frac{1}{2}]$ symmetry point between the TO and TA phonons ($64.7+52.5\approx 117 cm^{-1}$) and the $\Sigma[\frac{1}{2},\frac{1}{2},0]$ point between the LO and T_1A phonons ($80+34\approx 114$ cm^{-1}) where we use the notation of Ref. 43 to designate the phonons. This band appears in the frequency region where the anharmonic effects are dominated by summation processes. This leads to our assignment of this band as a summation mode. The smaller sideband near 105 cm^{-1} may be assigned to the combinations at the

TABLE III. Lorentzian and void mode fit parameters used in the EMA dielectric function for the 1100-Å RbI film. Other parameters used in the model analysis include: $\epsilon_\infty=2.58$, thickness $=1082$ Å, and angle of incidence $= 85.8°–86.5°$. ω_{LO} values are determined from the peak positions of the $\mathrm{Im}(1/\epsilon)$ curves. ω_v values are determined from the FIRRAS spectra peak positions.

Lorentzian modes				Void modes				
ω_{LO} (cm^{-1})	ω_{TO} (cm^{-1})	γ (cm^{-1})	S (cm^{-2})	ω_v (cm^{-1})	L	f	Vol. (%)	c/a
			87 K					
105.5	80.2	5.5	12 300	96.5	0.65	0.5	7.0	0.32
	106.0	5.5	10	83.5	0.95	0.5		0.07
	110.0	6.0	75					
			144 K					
103.5	79.0	7.0	11 675	93.5	0.65	0.5	6.5	0.32
	104.0	5.5	50	81	0.95	0.5		0.07
	109.0	7.0	65					
			183 K					
101	78.0	9.0	11 250	93	0.55	0.4	5.0	0.46
105	104.0	6.0	60	79	0.95	0.6		0.07
112	112.0	7.5	75					
			223 K					
100.5	77.0	10.5	11 200		0.55	0.5	5.0	0.46
104	105.0	6.5	50	79.5	0.95	0.5		0.07
111.5	112.0	7.0	100					
			300 K					
99	75.5	13.3	11 400		0.55	0.5	5.0	0.46
104.5	104.0	8.0	75		0.95	0.5		0.07
111.5	111.0	8.5	250					

$\Sigma[\frac{1}{2},\frac{1}{2},0]$ point between the LA and T_1A phonons ($62+34\approx96$ cm^{-1}) and the T_1A and T_2O phonons ($34+62\approx96$ cm^{-1}). The assignment for the smaller mode is less certain due to its small oscillator strength and proximity to the LO mode. These assignments are summarized for all samples in Table IV.

The motivation for considering sample morphology effects arises from the spectral features observed between ω_{TO} and ω_{LO} and the voids seen in the films in the SEM micrograph (Fig. 2). As discussed in Sec. II, the morphology of our samples is approximated by a solid film containing a small volume fraction of voids. The optical properties are modeled by constructing an effective dielectric function for the solid-void system. To make this model tractable, we make some assumptions about the shape, orientation, and distribution of the voids:

(1) The voids have an ellipsoidal shape, specifically, that of an ellipsoid of revolution; (2) the axes of revolution of the ellipsoids are parallel to one another and to the incident **E** field; and (3) the total proportion of void volume is small ($<10\%$ in most cases) compared to the total volume of the film.

The shape of the ellipsoid determines the value of the depolarization factor L.[44] The volume fractions f_i, and depolarization factors L_i for each void shape, along with the bulk dielectric function, fully determine the effective dielectric function given by Eq. (4).

We found in Eq. (6) that each different void shape will give rise to an absorption peak at a frequency ω_{Vi}, where $\omega_{TO}<\omega_{Vi}<\omega_{LO}$. These void resonances are clearly visible in our spectra at lower temperatures (see Fig. 3). The widths of these void resonances follow the width of the lattice LO mode. As the temperature increases, the widths of the void resonances increase along with the width of the LO mode. At room temperature, they are only discernable as an asymmetry on the low-frequency side of the LO mode.

The parameters for each void resonance are obtained from the lowest-temperature spectra, since this is where they are most distinct. The calculated peak position is

TABLE IV. Summation-band assignments.

Observed summation bands (cm^{-1})	Assignments Symmetry point	Combinations (cm^{-1})
	RbI ($\omega_{LO}=99$ cm^{-1})	
104.5	$\Sigma[\frac{1}{2},\frac{1}{2},0]$	$LA+T_1A$ ($62+34\approx96$)
		T_1A+T_2O($34+62\approx96$)
111.5	$L[\frac{1}{2},\frac{1}{2},\frac{1}{2}]$	$TO+TA$ ($64.7+52.5\approx117$)
	$\Sigma[\frac{1}{2},\frac{1}{2},0]$	$LO+T_1A$ ($80+34\approx114$)
122	$L[\frac{1}{2},\frac{1}{2},\frac{1}{2}]$	$TO+LA$ ($64.7+64.7\approx129.5$)
	$\Sigma[\frac{1}{2},\frac{1}{2},0]$	$LA+T_2O$ ($62+62\approx124$)
	RbBr ($\omega_{LO}=122$ cm^{-1})	
134.5	$L[\frac{1}{2},\frac{1}{2},\frac{1}{2}]$	$TA+TO$ ($69+69\approx138$)
	KI ($\omega_{LO}=131$ cm^{-1})	
148.5	$L[\frac{1}{2},\frac{1}{2},\frac{1}{2}]$	$TO+TA$ ($98+55\approx153$)
156.5	$L[\frac{1}{2},\frac{1}{2},\frac{1}{2}]$	$TO+LA$ ($98+69\approx167$)
	CsI ($\omega_{LO}=90$ cm^{-1})	
82[a]	$\Sigma[\frac{1}{2},\frac{1}{2},0]$	Combinations of Σ_1,Σ_4
94.5		at 44.5 cm^{-1}, and Σ_3 at
98.5		43 cm^{-1}
	CsBr ($\omega_{LO}=116.5$ cm^{-1})	
104[b]	$\Sigma[\frac{1}{2},\frac{1}{2},0]$	T_2A+LA ($53.6+53.6\approx107$)
122	$L[\frac{1}{2},\frac{1}{2},\frac{1}{2}]$	$TA+LA$ ($62+62\approx124$)
140	$L[\frac{1}{2},\frac{1}{2},\frac{1}{2}]$	(TA,TO)+(LA,LO)
		($62+81\approx141$)

[a]This band is due in part to a void resonance.
[b]This band is due in part to a void resonance.

sensitive to the choice of the depolarization factor L_i, as expected from Eq. (6). The peak position is much less sensitive to the choice of volume fraction for the void. The peak height of the void resonance is fit by adjusting f_i. Table III summarizes the parameters obtained for the void resonances for the 1100-Å RbI sample. In Table III, c/a are the axial ratios of the voids corresponding to the appropriate depolarization factor L, taken from Osborn.[44] The c axes of the ellipsoids are perpendicular to the film surface. The total volume of the voids in the thicker films (see Table V) is less than 7%. This is in reasonable agreement with the density measurements performed on RbI films. As the temperature is increased, the sample morphology had a less noticeable effect on the spectra. The void parameters do not change significantly from their low-temperature values, with the exception of the total volume fraction, which decreased as the temperature increased. This follows from considering the

TABLE V. Void mode fit parameters used in the EMA dielectric function at 85 K for all the films studied. ω_{LO} values are determined from the peak positions of the $\mathrm{Im}(1/\epsilon)$ curves. ω_v values are determined from the FIRRAS spectra peak positions.

ω_{LO} (cm^{-1})	ω_v (cm^{-1})	L	f	Vol. (%)	c/a
		2500 Å RbI			
106.5	95.1	0.75	1.0	0.7	0.20
		1100 Å RbI			
105.5	96.5	0.65	0.5	7.0	0.32
	83.5	0.95	0.5		0.07
		350 Å RbI			
104	95	0.60	1.0	6.0	0.38
		210 Å RbI			
105.5	95.5	0.60	1.0	7.0	0.38
	83				
		120 Å RbI			
101.5	93	0.45	0.5	11.0	0.66
	84.5	0.64	0.5		0.33
		60 Å RbI[a]			
98	93.5	0.48	1.0	20.0	0.58
	84				
		60 Å RbI[b]			
96.5	91.5	0.34	1.0	40.0	0.96
	79.5				
		700 Å KI			
140.5	129	0.65	1.0	2.0	0.32
		570 Å RbBr			
128.5	118.5	0.55	0.8	6.0	0.46
	107	0.85	0.2		0.11
		700 Å CsI			
92.5	82.5	0.63	0.7	8.0	0.33
	72	0.90	0.3		0.07
		670 Å CsBr			
116.5	107.5	0.50	0.9	9.0	0.55
	96.5	0.78	0.1		0.17
		3270 Å CsBr			
118	107	0.55	1.0	2.3	0.46

[a]Before 12 h exposure to atmosphere.
[b]After 12 h exposure to atmosphere.

volume expansion of the film—as the film is heated, the islands that make up the film expand, reducing the volume of the voids. The linear expansion coefficients of RbI,[45] aluminum, and glass[46] are approximately 35.2×10^{-6} K^{-1}, 23×10^{-6} K^{-1}, and 9×10^{-6} K^{-1}, respectively, in the temperature range of interest. Taking the expansion of the aluminized glass substrate into account, the volume of the RbI film increases by approximately 1% between 85 and 300 K. This compares reasonably well with the reduction in void volume of 2% in the 1100-Å RbI film for this temperature change (see Table III). The spectral fitting was relatively insensitive to small changes in void volume at higher temperatures (> 200 K), where the void volume and shape parameters were used to fit the asymmetry of the low-frequency side of the LO mode. Because of this insensitivity to the void volume parameter at higher temperatures, the relative agreement in the magnitude of the change of the volume parameter may not be that significant. Indeed, different thicknesses of RbI and films of other materials show no apparent change in the volume parameter with temperature; or, in the case of the cesium halides, show an increase in void parameter with temperature. This is indicative of the difficulty of quantitatively comparing the void parameters with the actual film morphology, as discussed below. In the case of the cesium halides, the low-frequency feature seen at all temperatures may be due to a combination of a void resonance and a two-phonon absorption.

A detailed interpretation of the values in Table III is difficult without an independent quantitative characterization of the film's sample morphology. The analysis of the FIRRAS spectra gives the depolarization factors and axial ratios for the two shapes of voids that would give void resonances at the frequencies shown. One is an almost round spheroid ($\omega_{V1}=96.5$ cm^{-1}, $L_1\approx0.65$, $c/a_{(1)}\approx0.32$) and the other is a rather flat oblate spheroid ($\omega_{V2}=83.5$ cm^{-1}, $L_2\approx0.95$, $c/a_{(2)}\approx0.07$). From the nucleative nature of the growth of these films, the first shape would be a reasonable one to expect to be in the bulk of the film and contribute to the FIRRAS spectra. The relatively smooth film surfaces, shown by the scanning-electron-microscopy and atomic-force-microscopy analyses, may give rise to the feature attributed to the flat oblate spheroidal shapes. It is difficult to fit the lowest-frequency features (i.e., $\omega_{V2}=83.5$ cm^{-1}) with the void parameters, since the calculated FIRRAS spectra was relatively insensitive to changes in the depolarization factor L_2 close to 1.

The effects of changing morphology were seen in a 60-Å-thick RbI film inadvertently exposed to the (damp) atmosphere. In Fig. 5 we show 84-K FIRRAS spectra before and after the film had been exposed to atmosphere for 12 h. Since the film is hygroscopic, we expect prolonged exposure to the atmosphere to produce both a larger number of voids and/or an increase in the volume of the existing voids. The spectra obtained before exposure are modeled with an EMA dielectric function with a volume fraction of 10% and 20% voids at 300 and 82 K, respectively. The spectra obtained after exposure were modeled with a volume fraction of 20% and 40% voids

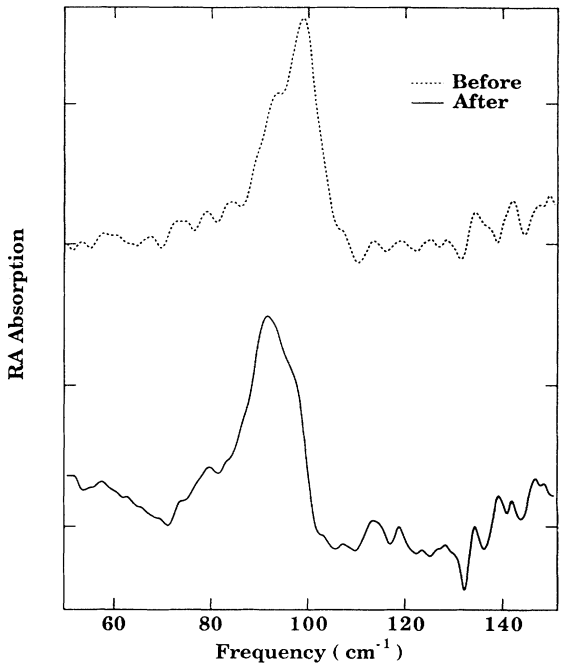

FIG. 5. 84-K FIRRAS spectra of 60-Å film before (dotted line) and after (solid line) 12 h exposure to laboratory air.

at 300 and 84 K, respectively. As the fraction of voids increases, the void resonances become more dominant, as seen in Fig. 5. It is this increase in the void resonance and the attendant decrease in the LO resonance that appears to shift the LO mode to lower frequencies in the exposed 60-Å film.

In addition to the effects of sample morphology, we have studied the effects of sample thickness on the lattice dynamics. The room-temperature LO-mode frequencies for the different RbI film thicknesses are shown in Tables II and VI. The LO-mode frequency remains constant at 99 cm^{-1} for films thicker than 350 Å, decreasing rapidly below 350 Å to 90.5 cm^{-1} at 60 Å. A reduction of the mode strength with film thickness is also seen and is a result of the smaller atomic force constants at the surface of the film. Da Costa and Coleman[4] have shown that the frequency of the peak in the FIRRAS spectra depends on the oscillator strength of the mode. Therefore, as the oscillator strength decreases with thickness, the LO-mode

TABLE VI. LO-phonon frequency and mode strength as a function of thickness for RbI.

Thickness (Å)	ω_{LO} (cm^{-1})	Mode strength (cm^{-2})
2500	99	12 000
1100	99	11 400
350	98	10 500
210	98	10 900
120	95.5	9700
60	90.5	7500

frequency decreases as well (see Table VI). Bruesch *et al.*[47] have shown that the LO-mode frequency in thin sputtered films of Al_2O_3 depends on the thickness of the film. Bruesch *et al.* argue that the restoring forces acting on the atoms at the surface are smaller than those acting on the atoms in the bulk. We see a similar effect in RbI at much larger film thickness than in Al_2O_3, which is due to the long-range Coulomb forces in the more ionic RbI.

For thick films (2500 Å), the measured LO-mode frequency at 300 K is 99 cm^{-1} (see Table II). There is an additional feature at 122 cm^{-1} that is not observed in thinner films. We assign this mode to a combination of two-phonon summation processes between the TO and LA phonons at the $L[\frac{1}{2},\frac{1}{2},\frac{1}{2}]$ symmetry point ($64.7+64.7\approx129.5$ cm^{-1}) and the LA and T_2O phonons at the $\Sigma[\frac{1}{2},\frac{1}{2},0]$ symmetry point ($62+62\approx124$ cm^{-1}).[43] A greater number of high-frequency summation bands are observed in the thicker films. This is especially noticeable in the 2500-Å RbI film (Fig. 6). This is an example of the increased enhancement of the high-frequency sidebands due to the increase in oscillator strength with thickness.

A summary of our analyses of a range of RbI films is presented in Tables II, V, and VI. A more-detailed discussion of these results appears elsewhere.[5]

B. Other Materials

We have examined thin films of four other alkali halides: Potassium iodide (700 Å), rubidium bromide (570 Å), cesium iodide (700 Å), and cesium bromide (670 and ~3270 Å). A summary of our results appears in Tables II, IV, and V.

There is some ambiguity in the assignments of the satellite bands in the cesium halides. The low-frequency satellite bands due to sample morphology are observed at low temperature, but one of the bands (82 cm^{-1} in CsI and 104 cm^{-1} in CsBr) can also be assigned to summation processes (see Table IV). Lowndes reports a similarly shaped $\mathrm{Im}(1/\epsilon)/\omega$ curve for his bulk reflectance measurement of CsI (Ref. 36) at room temperature. This would suggest the assignment of the low-frequency features to two-phonon summation bands rather than thin-film sample morphology. The presence of these particular bands at low temperature, where the other summation bands have disappeared, however, makes this assignment somewhat unclear.

The frequency shift with temperature of the LO mode is markedly different between the rubidium halides (~6 cm^{-1}) and potassium iodide (~10 cm^{-1}) compared to that in the cesium halides (~2 cm^{-1}) (see Tables II and V). The shift of the TO- and LO-mode frequencies with temperature is due to lattice thermal expansion and anharmonic interactions. The portion of the frequency shift due to the anharmonic interactions is negative in the rubidium halides and potassium iodide and positive in the cesium halides studied here. This accounts for the difference in the observed frequency shifts.[38,52]

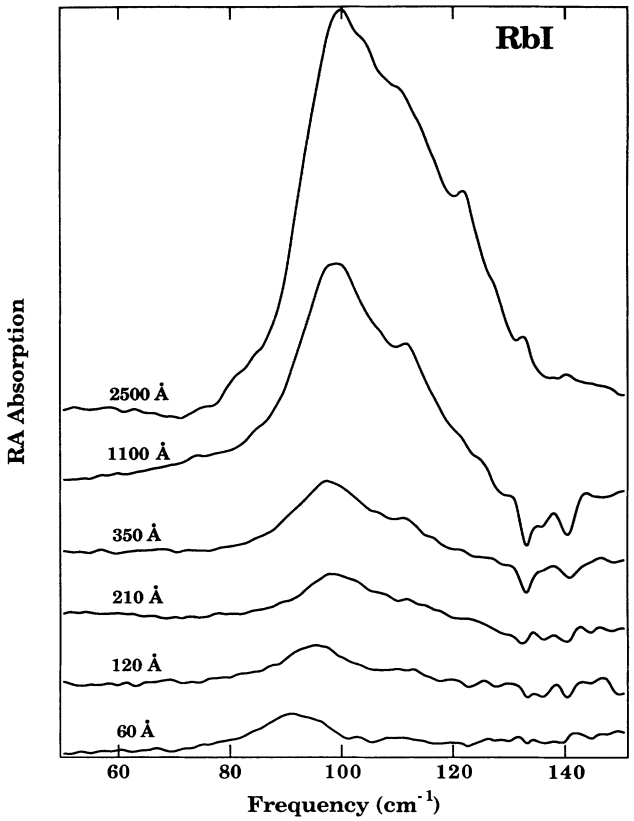

FIG. 6. Film-thickness dependence of room-temperature FIRRAS spectra of RbI. Spectra are displayed for clarity.

We have demonstrated that FIRRAS shows promise as a nondestructive thin-film characterization technique as well as a probe of lattice dynamics in thin films. Since the data presented in this paper were gathered, we have extended the range of the FIRRAS spectrometer to 340 cm^{-1} and the accessible temperature range to 15 K.[53] These modifications will enable us to study a wider variety of materials.

[1]V. M. Da Costa, Ph.D. thesis, University of California at Davis, 1988 (unpublished).
[2]V. M. Da Costa and L. B. Coleman, Rev. Sci. Instrum. **61**, 2113 (1990).
[3]V. M. Da Costa and L. B. Coleman, Appl. Spectrosc. **44**, 1301 (1990).
[4]V. M. Da Costa and L. B. Coleman, Phys. Rev. B **43**, 1903 (1991).
[5]T. G. Fiske, Ph.D. thesis, University of California at Davis, 1990 (unpublished).
[6]T. G. Fiske and L. B. Coleman, Bull. Am. Phys. Soc. **35**, 498 (1990).
[7]D. W. Berreman, Phys. Rev. **130**, 2193 (1963).
[8]R. G. Greenler, J. Chem. Phys. **44**, 310 (1966).
[9]D. W. Berreman, Phys. Rev. **163**, 855 (1967).
[10]C. A. Fenstermaker and F. L. McCrackin, Surf. Sci. **16**, 85 (1969).
[11]D. W. Berreman, Phys. Rev. B **1**, 381 (1970).

[12]D. W. Berreman, J. Opt. Soc. **60**, 499 (1970).
[13]I. Ohlidal and F. Lukes, Opt. Acta **19**, 817 (1972).
[14]W. L. Schaich and W. Chen, Phys. Rev. B **39**, 10 714 (1989).
[15]W. Chen and W. L. Schaich, Surf. Sci. **218**, 580 (1989).
[16]D. Polder and J. H. Van Santen, Physica **12**, 257 (1946).
[17]D. E. Aspnes, J. B. Theeten, and F. Hottier, Phys. Rev. B **20**, 3292 (1979).
[18]F. L. Galeener, Phys. Rev. Lett. **27**, 1716 (1971).
[19]F. L. Galeener, Phys. Rev. Lett. **27**, 421 (1971).
[20]L. Genzel and T. P. Martin, Phys. Status. Solidi B **51**, 91 (1972).
[21]L. Genzel and T. P. Martin, Surf. Sci. **34**, 33 (1973).
[22]A. S. Barker, Phys. Rev. B **7**, 2507 (1973).
[23]R. W. Cohen, G. D. Cody, M. D. Coutts, and B. Abeles, Phys. Rev. B **8**, 3689 (1973).
[24]*Electrical Transport and Optical Properties of Inhomogeneous Media,* edited by J. C. Garland and D. B. Tanner (AIP, New York, 1978).
[25]R. Landauer, in *Electrical Transport and Optical Properties of Inhomogeneous Media,* edited by J. C. Garland and D. B. Tanner (AIP, New York, 1978), p. 2.
[26]C. G. Granqvist and O. Hunderi, Phys. Rev. B **18**, 2897 (1978).
[27]D. Stroud, Phys. Rev. B **12**, 3368 (1975).
[28]S. A. FitzGerald *et al.*, Phys. Rev. B **42**, 5469 (1990).
[29]R. Ruppin and R. Englman, Rep. Prog. Phys. **33**, 149 (1970).
[30]W. L. Bragg and A. B. Pippard, Acta Crystallogr. **6**, 865 (1953).
[31]T. G. Fiske, V. M. Da Costa, and L. B. Coleman, Rev. Sci. Instrum. **62**, 1861 (1991).
[32]R. G. Greenler, J. Chem. Phys. **50**, 1963 (1969).
[33]J. D. McIntyre and D. E. Aspnes, Surf. Sci. **24**, 417 (1971).
[34]H. Ibach, Surf. Sci. **66**, 56 (1977).
[35]R. P. Lowndes and D. H. Martin, Proc. R. Soc. London, Ser. A **308**, 473 (1969).
[36]R. P. Lowndes, Phys. Rev. B **1**, 2754 (1970).
[37]K. F. Pai *et al.*, Infrared Phys. **18**, 199 (1978).
[38]P. Bruesch, *Phonons: Theory and Experiments I* (Springer-Verlag, Berlin, 1982).
[39]J. R. Hardy and A. M. Karo, *The Lattice Dynamics and Statics of Alkali Halide Crystals* (Plenum, New York, 1979).
[40]J. E. Eldridge, Phys. Rev. B **6**, 1510 (1972).
[41]J. E. Eldridge and K. A. Kembry, Phys. Rev. B **8**, 746 (1973).
[42]E. Burstein, F. A. Johnson, and R. Loudon, Phys. Rev. **139**, A1239 (1965).
[43]G. Raunio and S. Rolandson, Phys. Status. Solidi **40**, 749 (1970).
[44]J. A. Osborn, Phys. Rev. **67**, 351 (1945).
[45]G. K. White, Proc. R. Soc. London, Ser. A **286**, 204 (1965).
[46]R. Resnick and D. Halliday, *Physics* (Wiley, New York, 1977).
[47]P. Bruesch, R. Kotz, H. Neff, and L. Pietronero, Phys. Rev. B **29**, 4691 (1984).
[48]G. Dolling, R. A. Cowley, C. Schittenhelm, and I. M. Thorson, Phys. Rev. **147**, 577 (1966).
[49]S. Rolandson and G. Raunio, J. Phys. C **4**, 958 (1971).
[50]W. Buhrer and W. Halg, Phys. Status Solidi B **46**, 679 (1971).
[51]S. Rolandson and G. Raunio, Phys. Rev. B **4**, 4617 (1971).
[52]R. P. Lowndes and A. Rastogi, Phys. Rev. B **14**, 3598 (1976).
[53]G. J. R. Spooner and L. B. Coleman, Bull. Am. Phys. Soc. **35**, 447 (1990).

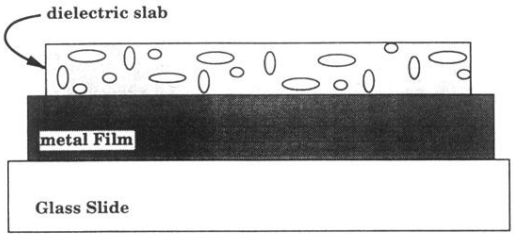

FIG. 1. Schematic representation of film samples with ellipsoidal voids.

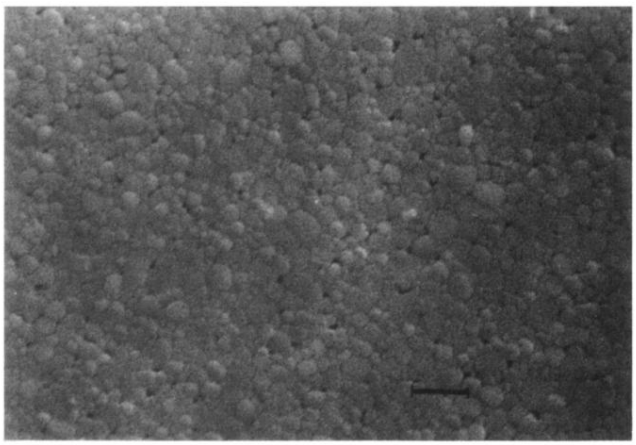

FIG. 2. Scanning electron micrograph of RbI film. Magnification is times 11 380. Bar represents 8790 Å.